Biomedical Microdevices (2020) 22: 73
https://doi.org/10.1007/s10544-020-00525-0

# A ten-minute, single step, label-free, sample-to-answer assay for qualitative detection of cytokines in serum at femtomolar levels

Pengfei Xie[1] · Naixin Song[2] · Wen Shen[2] · Mark Allen[2] · Mehdi Javanmard[1]

Accepted: 22 September 2020 / Published online: 10 October 2020


## Abstract

Label-free electronic affinity based immuno-sensing is an attractive candidate as a platform technology for analyzing biomarkers due to the ease of miniaturization and minimal use of reagents. Electronic based sensing approaches, however, have lagged behind their optical counterparts in terms of detection limit, selectivity, and reliability. Also, the matrix dependent nature of electronic sensing modalities makes difficult the analysis of biomarkers in high salt concentration samples such as serum due to charge screening. We present a novel sensing platform, the micro-well sensor, that works by functionalizing nanoscale volume wells with antibodies and monitoring the impedance change inside the wells due binding of target protein. This detection modality is advantageous to many label-free electronic sensors in that signal power scales with increase in salt concentration, thus improving the sensitivity of the platform. We demonstrate rapid label-free qualitative detection of cytokines within ten minutes at femtoMolar concentrations and a dynamic range of 3 orders of magnitude in serum samples. We describe the design, fabrication, and characterization of the micro-well sensor in serum samples using inflammatory protein biomarkers.

**Keywords** Label-free biosensors · Cytokine quantifications · Impedance detection · Protein detection · Proteomics · Biomarker detection · Diagnostics

## 1 Introduction

Affinity based biosensors detect proteins and nucleic acids through immobilization of probe molecules on a transducer substrate to attain specificity in detection of the target macromolecule of interest. In the context of protein detection, protein array technologies provide a valuable platform for functional proteomic analysis (Ray et al. 2010). A protein microarray provides a multi-functional platform enabling comprehensive and high throughput studies, which can be widely used in biomarker validation studies (Hudson et al. 2007), study of protein–protein interactions (Schweitzer et al. 2003), protein–DNA interactions (Kersten et al. 2004), and detection of various antigens and antibodies (Chamritski et al. 2007). Among affinity-based biosensing technologies, there are two major detection strategies, label-based and label-free. Both approaches have their merits and disadvantages. Label-based technologies typically achieve lower detection limits and higher selectivity, yet require multiple steps. Label-free techniques tend to lag behind their labeled counterparts in terms of detection limit and specificity, yet often can be performed in a single step, while also enabling real-time monitoring and determination of the binding kinetics involved in the interaction (Yu et al. 2006; Haab 2003).

Label-free biosensing technologies, both optical and electrical, have shown significant promise in the research setting and in the literature (Zheng et al. 2005a; Armani et al. 2007), however, have had difficulty moving beyond the lab and progressing to commercialization, or more importantly clinical translation. (Sin et al. 2014; Luong et al. 2008) In the context of protein biomarker detection, exceptions include plasmonic based technologies like BIAcore (Fivash et al. 1998) and photonic technologies such as BioLayer interferometry (Concepcion et al. 2009). IonTorrent, a commercially available label-free electronic CMOS based technology for DNA sequencing, has shown promise for relatively low cost genome sequencing (Eisenstein 2010). The ability to accurately assay biological samples to the extent where it can be used for reliably attaining measurements in animal or human

**Electronic supplementary material** The online version of this article (https://doi.org/10.1007/s10544-020-00525-0) contains supplementary material, which is available to authorized users.

✉ Mehdi Javanmard
mehdi.javanmard@rutgers.edu

[1] Rutgers University, New Brunswick, NJ, USA

[2] University of Pennsylvania, Philadelphia, PA, USA

studies requires minimizing measurement inconsistency, device variability, and also must be capable of accurate detection of biomarkers in biological matrices like blood, which is highly complex and has high salt concentration. Electronic detection technologies, such as charge based sensing using nanowire FETs and impedance sensing based on double layer modulation, often operate effectively in low salt environments (Zheng et al. 2005a; Gao et al. 2015; Esfandyarpour et al. 2013). High salt concentration results in charge screening and minimizing the double layer thickness to approximately 1 nm, thus making E-fields unable to penetrate beyond the length of the capture antibody (10–20 nm). A novel approach based on incorporating a porous biomolecule permeable layer on the sensor which increases the effective screening length in the region immediately adjacent to the device has also been presented (Gao et al. 2015). Using this approach, they detected Prostate Specific Antigen in 100 mM Phosphate Buffer at a detection limit of 10 nM. The primary challenge faced by label-free technologies stems from measurement variability and inconsistency, thus not being suitable for reliable quantification of molecular levels. The first and foremost reason is that stochastic variations in levels of binding greatly increase as biosensors excessively miniaturize down to the nanoregime (Das et al. 2009). The probability of diffusion of the analyte and its subsequent binding to the sensor surface decreases significantly when the sensor active area dimensions are in the nano-regime. Hassibi et al. (Das et al. 2009) developed a comprehensive noise model examining the effects of scaling on the solution to the Fokker-Planck equation and analyte binding fluctuation, and demonstrated that scaling down significantly reduces the achievable repeatability and dynamic range of biosensors. This can potentially explain one of the reasons why technologies such as BIAcore (Myszka et al. 1998), BioLayer Interferometry (Concepcion et al. 2009), and IonTorrent (Merriman et al. 2012), which are all microscale detection technologies, have been successfully commercialized while nanoscale label-free technologies, such as nanowires (Zheng et al. 2005b) and Surface Enhanced Raman Scattering (Han et al. 2009; Fabris et al. 2008), have had difficulty making it out of the lab, despite the promise they have shown in the literature. The problem of inconsistency is even more pronounced in nano-sensors that have been fabricated using bottom-up synthesis approaches (Liu and Lee 2005; Choi et al. 2010; Liu et al. 2007), that show great sensitivity, yet repeatability is a major problem resulting from batch to batch fabrication variations. Thus, top-down fabrication approaches have shown promise to work with higher precision (Duan et al. 2012). Probe-free detection modalities, such as Surface Enhanced Raman Scattering (SERS), are highly dependent not only on the binding rate of molecules with the sensor surface, but also the orientation of the binding analyte (Yu and Golden 2007), thus inconsistency is an issue even for precisely patterned sensors using top-down fabrication approaches. Label-free sensing approaches have also lagged behind their fluorescence-label based counterparts due to lack of long-term reliability resulting from electrode corrosion and fowling. Additionally, nanopore based sensing is an established method for achieving extremely high sensitivity, even at physiological salt concentrations. Functionalized nanopores have been shown to achieve selectivity in protein detection (Actis et al. 2010; Umehara et al. 2009). Label-free protein sensing with low detection limits has been demonstrated using nanotextured materials (Jacobs et al. 1690, 2014; Panneer Selvam and Prasad 2013; Selvam et al. 2012). Detection of proteins in blood or serum using label-free impedance based techniques is difficult due to high salt concentration of the matrix, which results in screening of the charge of the target proteins. Numerous label-free impedance based techniques have been developed over the last several decades which for the most part involve charge and capacitive based measurements (Daniels and Pourmand 2007; Lee et al. 2008; Maalouf et al. 2007), which are sensitive to salt concentration of the matrix and its effect on the charge screening debye length (Shanmugam et al. 2016; Chang and Park 2010; Prodromidis 2010). Novel sensors have also been developed using two dimensional materials and other novel materials (Kamakoti et al. 2016; Sarkar et al. 2014). Recent progress has been made by several groups demonstrating detection of cardiac and cancer biomarkers (Tuteja et al. 2016; Chikkaveeraiah et al. 2012). In this work, we describe a novel sensing configuration based on resistive sensing using standard non-faradaic electrodes where sensitivity is enhanced as the salt concentration of the matrix increases. No microparticles, nanoparticles, or electrochemical redox reagents are needed to enhance sensitivity and detection is performed in a single step. We demonstrate robust performance through repeated testing in rat serum.

### 1.1 Micro-well Array impedance sensor

The micro-well impedance sensor consists of a pair of overlapping electrodes with a thin dielectric layer sandwiched in between (Fig. 1). An array of wells embedded into the overlapping area creates a conductive path between the top electrode and bottom electrode. Probe antibodies are immobilized inside the wells. The impedance between the two electrodes is monitored in real-time. As proteins bind to the antibodies inside the wells, the impedance between the two electrodes increases. This increase is due to the partial occlusion of ions passing between the electrodes. The quantity of target protein present in the serum will determine the ultimate drop in current measured between the electrodes. Higher salt concentration results in larger current, thus higher signal power corresponding to larger changes in current due to protein binding, making the sensor ideal for quantification of proteins in high salt content matrices such as serum. The sensor consists of a

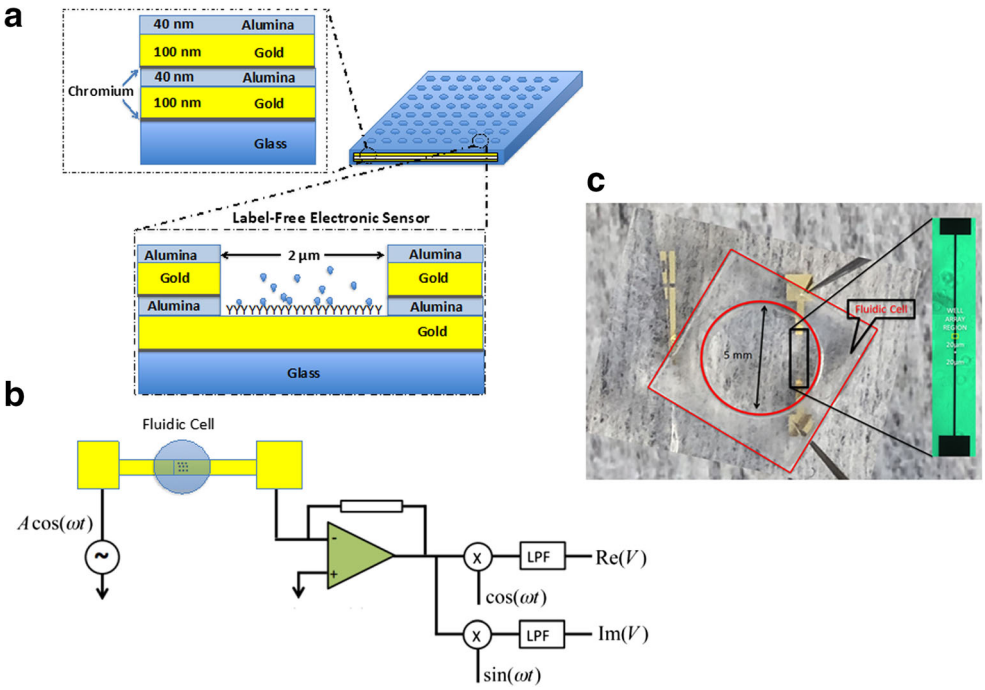


**Fig. 1** **a** Micro-well Array Label-free Impedance sensor schematic. Electrodes in the array monitor impedance in the well. As protein binds to antibodies functionalized in the well, a rise in impedance is observed between electrodes. **b** Measurement setup using lock-in-amplifier

stack of two gold electrodes in which the bonding pads accessing each are located on opposite sides of the chip. The two electrodes extend from the bonding pads to the center of the chip such that they overlap each other with an area of 20 µm × 20 µm. Lock-in-amplification is used to measure the AC current passing through the electrodes inside the wells.

## 2 Materials and methods

### 2.1 Sensor fabrication

The following fabrication procedure was used to form the sensors on a glass substrate. The first electrode was fabricated using standard photolithography, electron beam evaporation of gold, and lift-off processing. The metal layer consists of a 5 nm layer of chromium for enhancing adhesion of the gold film to the substrate and a 100 nm gold layer on top. A 40 nm layer of aluminum oxide is deposited onto the first electrode using atomic layer deposition. The second electrode layer (again consisting of 5 nm chromium and 100 nm gold) is patterned using the same procedure as the first layer. Another 40 nm layer of aluminum oxide is deposited on top of the second electrode using atomic layer deposition to serve as a protection against fouling. A layer of photoresist is spin coated onto the wafer. An array of micron-sized holes is photo-patterned onto the overlapping area of the two electrodes. Multiple wet etch steps are performed to remove the top aluminum oxide layer (buffered oxide etchant), the gold and chromium layer (gold and chromium etchant), and the bottom aluminum oxide layer (buffered oxide etchant) inside the wells. The photoresist is then stripped off. A second photomask is used to pattern photoresist to protect the sensors to be able to etch off various parts of the alumina outside of the sensing region to expose the glass surface. Devices with 20 µm × 20 µm and also 100 µm × 100 µm overlapping area are shown in Fig. 2a and b. Images of the devices were captured using an Ernst Leitz Wetzlar bright-field microscope (Fig. 2a) and a Zeiss Axio Imager M2M (Fig. 2b). A fluidic cell, for confining the liquid, made of PDMS was then bonded on top of the sensor substrate using oxygen plasma treatment. The fluidic cell consists of a millimeter diameter well that allows for fluid to be directly incubated onto the substrate.

### 2.2 Electrical impedance spectroscopy sensor characterization

It is critical to understand the impedance behavior of the system to determine the optimum frequency region for performing real-time measurements. We used a potentiostat (Gamry Instruments, Warminister, PA, USA) to characterize the impedance spectrum of the biosensor devices as shown in Fig. 2c. We performed impedance measurements on a multitude of fabricated sensors ranging from 10 Hz to 3 MHz. The impedance is dominated by the double layer capacitance until 100 kHz. Beyond 100 kHz, the impedance flattens out and becomes dominated by resistance. Thus we choose to operate at a frequency of 1 MHz, to monitor changes in ionic resistance as a result of antigen binding.

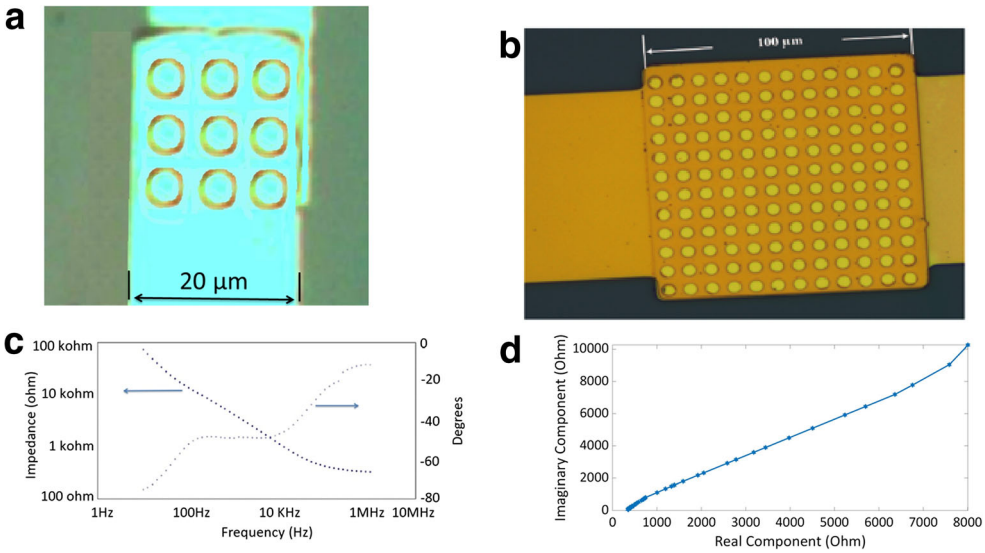


**Fig. 2** Microscopic images of micro-fabricated sensors of differing sizes and array size and density. **a** 9-well and **b** 144-well array device. **c** Magnitude and Phase of Impedance spectrum of device. **d** Nyquist curve of corresponding device. Device starts out capacitive at low frequencies and response becomes dominated by solution resistance as frequency is increased beyond 100 kHz. At 1 MHz, response is resistive which is the optimal regime of operation for the sensor. Accumulation of protein in micro-well results in increase in resistance between electrodes

### 2.3 Reagent preparation and antibody immobilization

Antibodies and target proteins were suspended in phosphate buffer saline (PBS). Monoclonal anti-human leptin IgG antibodies (MAB510, R&D Systems, Minneapolis, MN, USA) were suspended in PBS at a concentration of 0.2 mg/ml. The antibodies were physically adsorbed onto the sensor surface by injecting 5 µl of anti-leptin solution into the sensor well and incubating for 10 min. The target cytokine used in this study, human leptin (510RT, R&D Systems, Minneapolis, MN, USA), was suspended in concentrations ranging from 6 nM to 6 fM. All target cytokines including Leptin, Il6, Il4, and TNF-α were commercially purchased (R & D Systems, Minneapolis, Mn, USA). During experiments, the target cytokine buffer was mixed with pure rat serum at a 1:1. We spiked the target human cytokine (human leptin as opposed to rat leptin) in rat serum to test the effects of the background matrix on the sensor. This ensured that endogenous levels of rat leptin present in rat serum, would not interfere with the sensor during control experiments.

### 2.4 Real-time impedance measurements

Figure 4 shows a schematic describing our test setup. We formed a millimeter sized well on top of the sensor, confining the fluid. Reagents were sequentially added manually to the well, and the complex impedance was monitored in real time. The impedance inside the nano-wells is measured using a multi-frequency lock-in-amplifier (Zurich Instruments HF2IS, Zurich, SI). The AC excitation source, providing 0.4 V at a frequency of 1 MHz, was connected to one of the electrodes, and the second electrode was connected to the input of the lock-in-amplifier (gain of 1 k, bandwidth of 2 Hz, and sampling rate of 225 samples/s), where the real and imaginary component of the impedance were both acquired.

### 2.5 Statistical analysis

The percentage change in voltage was measured for each sensor in real time. Experiments were performed at each concentration in triplicate. Mean and standard deviation over the three measurements were calculated. The *p* value of the lowest measurable concentration (600 fM) with respect to the negative control experiments was calculated to assess statistical significance.

## 3 Results and discussion

### 3.1 Analysis of purified samples

To perform measurements with maximum sensitivity, it is extremely critical to capture impedance changes occurring in the sensors as biological binding events occur in real time. Tests were initially performed in purified samples. In Fig. S1, the output of the lock-in amplifier is shown as an empty well is filled with Phosphate Buffer Saline (PBS). The voltage at the output, or the current across the electrodes, increases by two orders of magnitude. This means the impedance across the electrodes decreases by two orders of magnitude, which is expected because of the high conductivity of the buffer. As a negative control, a blank PBS sample is added to the well, resulting in minimal shift in baseline in the positive direction (Fig. S2). In the next step, anti-leptin antibodies are added to the wells and the antibodies physically adsorb to the gold surface. Figure 3a shows representative data of the sensor response with respect to time as monoclonal antibody (anti-Leptin IgG) physically adsorbs in the channel resulting in

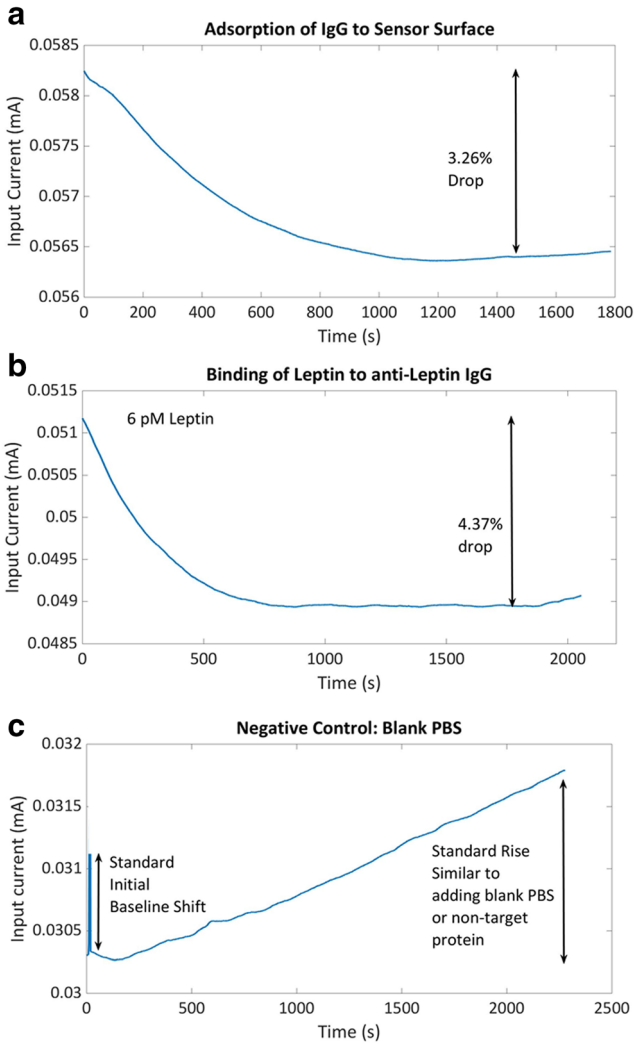


**Fig. 3** **a** Sensor response (absolute value of current across electrodes) with respect to time as monoclonal antibody (anti-Leptin IgG) physically adsorbs in channel resulting in exponential drop in baseline. **b** Sensor response (absolute value of current across electrodes) with respect to time as leptin in solution binds to electrode surface functionalized with anti-leptin IgG resulting in 4.37% drop in current across electrodes. **c** Negative control. When blank PBS sample is added in fluidic well containing sensor, aside from initial baseline shift common to all steps, current across electrodes generally rises by 1%. This is observed with all negative control experiments, likely due to antibody desorption

exponential drop in baseline. When the channel becomes filled with PBS, and antibodies are added to the mix and they adsorb inside the well, a decrease in output voltage or an increase in impedance is observed, which is consistent with our model, where the presence of protein results in occlusion of ionic current passing between the electrodes, thus resulting in an increase in resistance. Also, a unique exponential pattern to these drops in voltage (or rise in impedance) is observed, which is consistent with time dependent behavior of antigen antibody binding. This is similar to the response observed with surface plasmon resonance based biosensors (Piliarik et al. 2009). The time scale to reach saturation is on the order of ten to 15 min. Figure 3b describes the sensor response with respect to time as leptin in solution binds to electrode surface functionalized with anti-leptin IgG resulting in 4.37% drop in current across electrodes. The fluid in the well is then aspirated (Fig. S3) to remove extra antibodies in the solution, and PBS is re-injected (Fig. S4). Again, as a negative control, PBS is added on top of the existing solution. As a negative control, a blank solution of PBS is injected, resulting in a rise in current (drop in impedance is observed, likely due to desorption of antibodies) (Fig. 3c). For negative control experiments, the current across electrodes generally rises by 1%. This is seen with all negative control experiments and is likely due to antibody desorption. The addition of target antigen (Leptin) results in an exponential drop in current with a signature similar to that observed during antibody immobilization (Fig. 3b). Accumulation of protein due to non-specific binding results in an increase in the ionic resistivity inside the well. A non-target cytokine is injected into the well as a negative control. The current response is similar to that of the addition of blank PBS sample (Fig. S5). The relative change in impedance observed for each step is illustrated in Fig. 4.

### 3.2 Sensitivity and well size

After determining the optimum operation frequency and establishing functionality of the device, we set out to determine the optimum device geometry for detection of the protein binding in the well. We fabricated devices with micro-wells of different diameters. Figure 5 shows the results of repeated tests (in triplicate for each diameter) of varying well diameters. We observe that smaller diameter allows for larger normalized change in baseline impedance resulting from antibody adsorption inside the well compared to larger diameter wells. We also tested devices with oxide thicknesses of 30 nm and 40 nm to determine which provides better sensitivity. Devices with 40 nm spacing showed larger change in normalized impedance when antibody physically adsorbed inside the well compared to devices with 30 nm spacing. Since 40 nm thickness already provided a strong response, further testing was performed using 40 nm thick oxide devices with 2 μm diameter wells.

### 3.3 Spiked serum samples

Upon successful demonstration of sensor operation in purified samples and optimization of geometry, we quickly moved on to characterizing sensor performance in spiked serum samples. The procedure performed in all experiments for preparing and priming the sensors for the positive and negative control experiments is similar to that illustrated in Fig. 4. In all experiments, a negative control sample of serum from a healthy rat mixed with PBS (1:1 ratio) was used as a negative control showing response similar to that of blank samples. Rat

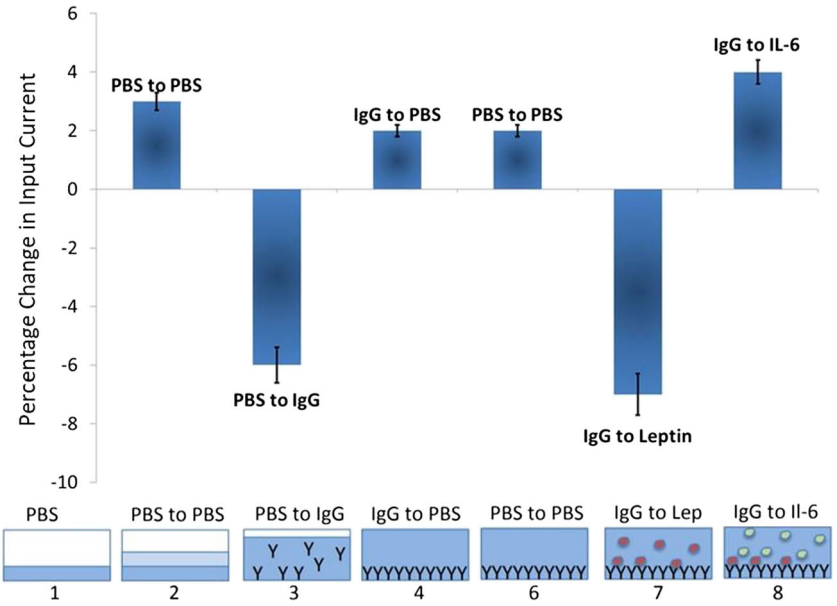


**Fig. 4** Illustration of experimental protocol for device validation with error bars (standard deviation over 3 experiments) and resulting percentage changes in impedance. Antibody adsorption and protein binding inside well results in decrease in impedance. Negative control steps (adding blank samples or non-targeted protein) results in positive change in current

serum (Sigma Aldrich, St. Louis, MO, USA) samples spiked with human leptin at a 1:1 ratio with PBS showed response similar to that of leptin in purified buffer.

### 3.4 Applicability to alternate target protein biomarkers

To showcase the agnostic nature of the platform technology and its utility to other target proteins and resilience to non-target proteins of higher abundance, we immobilized the sensor with alternate antibodies, including anti-TNF-α IgG (R & D Systems, Minneapolis, Mn, USA). Figure 6 shows representative data of the response obtained in rat serum when spiked both with (red curve) and without (Blue curve) the target antigen (TNF-α). In the negative control experiment (blue curve), we injected rat serum spiked with 1 nM of two non-target cytokines, rat Il6 and rat Il4, both, but no target protein (TNF-α). After the instantaneous baseline shift, the current rises, which is signature to all negative control experiments. In the positive test experiment (red), in addition to high background (1 nM) of non-target protein (rat Il6 and rat Il4), 1 pM of the target protein (rat TNF-α) was spiked in the rat serum. As seen (red curve), when the target protein (TNF-α) is present in the serum, the characteristic exponential decay over a period of minutes until reaching saturation is observed, whereas in the case of the negative control (red), the sensor reaches its minimum value within seconds and then begins rising (despite the high concentration of background rat Il4 and rat Il6). A third control experiment is performed (yellow curve) where only the target protein (TNF-α) is spiked in serum with no additional non-target proteins spiked. The result is similar to the first case where rat TNF-α and high background of non-target protein (rat Il6 and rat Il4) was spiked, in that the characteristic exponential decay over a period of minutes until reaching saturation is observed. This shows that the presence of high background of non-target proteins does not inhibit the sensors ability to detect target protein.

### 3.5 Dynamic range and detection limit characterization

A titration experiment was performed to determine sensor response as a function of analyte concentration. The

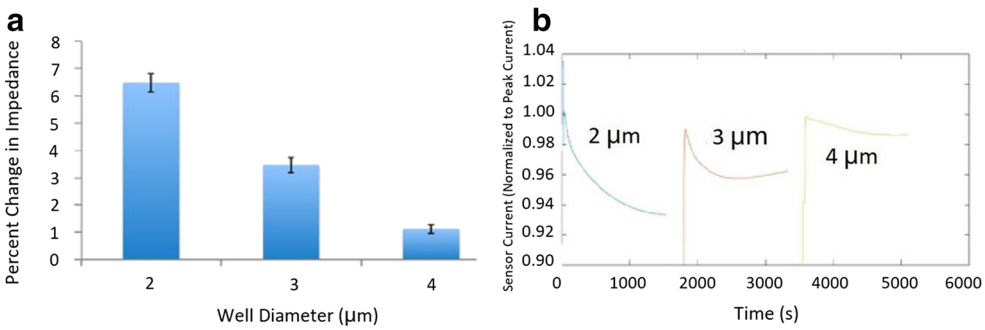


**Fig. 5** Relationship between sensor response (absolute value of current across electrodes) to protein binding and well diameter (Left) measured in triplicate over 3 different well sizes and (Right) the current across the electrodes verses time for 2 μm, 3 μm, and 4 μm diameter wells

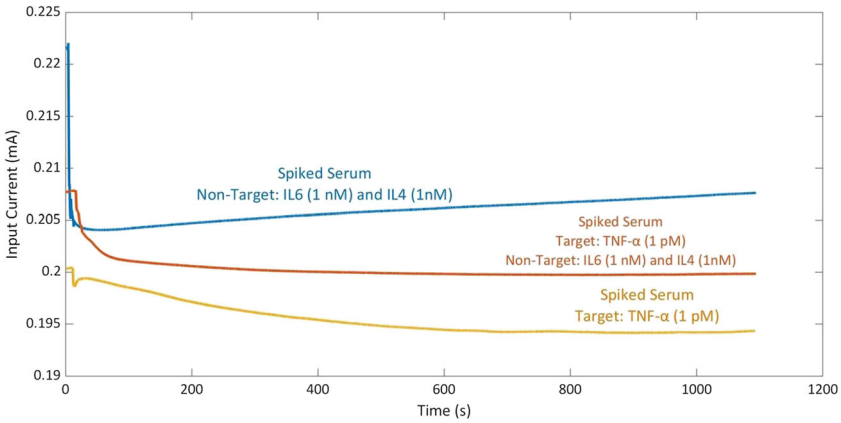


**Fig. 6** Sensor response (absolute value of current across electrodes) to the sample spiked with i) target protein (TNFα) at 1 pM and non-target proteins (Il6 and Il4) at 1 nM, ii) Negative control (serum spiked with non-target protein 1 nM of Il6 and TNFα), and iii) serum spiked only with target protein (TNFα) and no non-target proteins

concentration range tested included human leptin spiked into rat serum 60 pM all the way down to 6 fM. The titration curve for testing 2-μm diameter micro-well sensors is shown below in Fig. 7. Reliable detection of Leptin is shown 600 fM and higher. All negative control measurements were performed using non-spiked rat serum to ensure that sensor fouling did not result in false-positive signals. As seen in Fig. 7, the sensor has a dynamic range spanning 2 orders of magnitude (600 fM to 6 pM). All experiments were performed by spiking leptin into rat serum, and performed in triplicate.

## 4 Conclusion

We present a novel label-free biomolecular sensing modality that consists of an array of antibody functionalized nanoscale wells, embedded with electrodes for monitoring changes in ionic resistance as target protein binds inside the wells. The key novelty and advantage of this sensor geometry is that the high salt concentration of serum serves to improve the sensitivity of the system, as opposed to traditional label-free sensing approaches that work based on changes in capacitance or charge, which get limited by screening. High salt concentration increases the conductivity of the media, which increases the baseline signal power, thus improving overall signal to noise ratio. As a result, we were able to reliably and repeatedly detect target cytokines spiked in serum at concentrations as low as 600 fM with 2 orders of magnitude dynamic range within ten minutes. In a practical setting, a single step involving sample injection would be sufficient to perform sample to answer analysis using the micro-well sensor. This ease of use can enable a plethora of applications ranging from medical diagnostics to environmental monitoring and food safety. We emphasize that while we only demonstrated singleplex detection using leptin cytokine spiked in serum, the platform can be applied to a wide range of biomarkers. Multiplex analysis can be performed by fabricating an array of sensors, where each sensor is fabricated with antibodies targeting different proteins. A challenge with this assay in the current embodiment is the large error bars in the

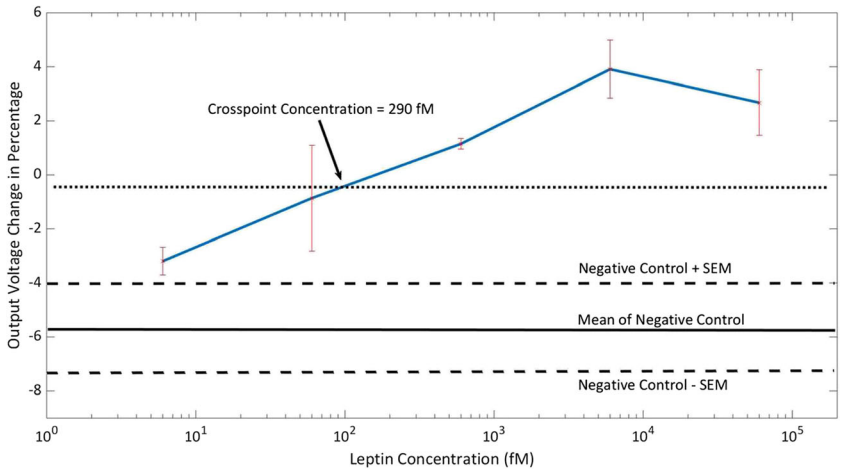


**Fig. 7** Titration curve for concentrations ranging from 60 pM down to 6 fM. Error bars are standard deviation over 3 points. Negative control (NC) is also included. Background level is defined where change in impedance across electrodes is no longer positive. Repeatable detection limit is 600 fM which is clearly above background. P-test was performed between 3 points obtained at 600 fM and 3 points obtained for negative control and resulted in a *P* value of 0.048 which is less than 0.05, which means the detection is statistically significant. 0% change crossing point is 290 fM. ANOVA analysis of all groups resulted in P value of 0.002 (P value <0.05), which indicates statistical significance

measurement. This can be improved by embedding multiple sensors in a single well plate and taking the average of multiple measurements. This can improve precision that may otherwise be hindered due to variations in device geometry during fabrication or the surface coverage of antibodies in each well. The readout electronics utilized in this study was a benchtop lock-in-amplifier, however, a miniaturized portable (Talukder et al. 2017) or wearable lock-in-amplifier (Furniturewalla et al. 2018) could be used instead with wireless transmission capabilities and readout on a smartphone.

**Acknowledgements** This work was sponsored by the Defense Advanced Research Projects Agency (DARPA) Biological Technologies Office (BTO) Electrical Prescriptions (ElectRx) program under the auspices of Dr. Eric Van Giesen through the DARPA Contracts Management Office Grant/Contract No HR0011-16-2-0026. The devices were fabricated using tools in the Rutgers Microelectronic Research Laboratory, Brookhaven National Laboratory Center for Functional Nanomaterials (special acknowledgement to Dr. Ming Lu), and University of Pennsylvania Singh Center for Nanotechnology.

## References

P. Actis, A.C. Mak, N. Pourmand, Functionalized nanopipettes: Toward label-free, single cell biosensors. Bioanal. Rev. **1**(2–4), 177–185 (2010)

A.M. Armani, R.P. Kulkarni, S.E. Fraser, R.C. Flagan, K.J. Vahala, Label-free, single-molecule detection with optical microcavities. Science **317**(5839), 783–787 (2007)

I. Chamritski, M. Clarkson, J. Franklin, S.W. Li, Real-time detection of antigen–antibody reactions by imaging ellipsometry. Aust. J. Chem. **60**(9), 667–671 (2007)

B.-Y. Chang, S.-M. Park, Electrochemical impedance spectroscopy. Annu. Rev. Anal. Chem. **3**, 207–229 (2010)

B.V. Chikkaveeraiah, A.A. Bhirde, N.Y. Morgan, H.S. Eden, X. Chen, Electrochemical immunosensors for detection of cancer protein biomarkers. ACS Nano **6**(8), 6546–6561 (2012)

D. Choi, Y. Choi, S. Hong, T. Kang, L.P. Lee, Self-organized hexagonal-nanopore SERS array. Small **6**(16), 1741–1744 (2010)

J. Concepcion, K. Witte, C. Wartchow, S. Choo, D. Yao, H. Persson, J. Wei, P. Li, B. Heidecker, W. Ma, Label-free detection of biomolecular interactions using BioLayer interferometry for kinetic characterization. Comb. Chem. High Throughput Screen. **12**(8), 791–800 (2009)

J.S. Daniels, N. Pourmand, Label-free impedance biosensors: Opportunities and challenges. Electroanalysis: An International Journal Devoted to Fundamental and Practical Aspects of Electroanalysis **19**(12), 1239–1257 (2007)

S. Das, H. Vikalo, A. Hassibi, On scaling laws of biosensors: A stochastic approach. J. Appl. Phys. **105**(10), 102021 (2009)

X. Duan, Y. Li, N.K. Rajan, D.A. Routenberg, Y. Modis, M.A. Reed, Quantification of the affinities and kinetics of protein interactions using silicon nanowire biosensors. Nat. Nanotechnol. **7**(6), 401–407 (2012)

M. Eisenstein, Life swallows ion torrent. Nat. Biotechnol. **28**(10), 994–994 (2010)

R. Esfandyarpour, M. Javanmard, Z. Koochak, H. Esfandyarpour, J.S. Harris, R.W. Davis, Label-free electronic probing of nucleic acids and proteins at the nanoscale using the nanoneedle biosensor. Biomicrofluidics **7**(4), 044114 (2013)

L. Fabris, M. Dante, T.Q. Nguyen, J.B.H. Tok, G.C. Bazan, SERS aptatags: New responsive metallic nanostructures for heterogeneous protein detection by surface enhanced Raman spectroscopy. Adv. Funct. Mater. **18**(17), 2518–2525 (2008)

M. Fivash, E.M. Towler, R.J. Fisher, BIAcore for macromolecular interaction. Curr. Opin. Biotechnol. **9**(1), 97–101 (1998)

A. Furniturewalla, M. Chan, J. Sui, K. Ahuja, M. Javanmard, Fully integrated wearable impedance cytometry platform on flexible circuit board with online smartphone readout. Microsystems & Nanoengineering **4**(1), 20 (2018)

N. Gao, W. Zhou, X. Jiang, G. Hong, T.-M. Fu, C.M. Lieber, General strategy for biodetection in high ionic strength solutions using transistor-based nanoelectronic sensors. Nano Lett. **15**(3), 2143–2148 (2015)

B.B. Haab, Methods and applications of antibody microarrays in cancer research. Proteomics **3**(11), 2116–2122 (2003)

X.X. Han, B. Zhao, Y. Ozaki, Surface-enhanced Raman scattering for protein detection. Anal. Bioanal. Chem. **394**(7), 1719–1727 (2009)

M.E. Hudson, I. Pozdnyakova, K. Haines, G. Mor, M. Snyder, Identification of differentially expressed proteins in ovarian cancer using high-density protein microarrays. Proc. Natl. Acad. Sci. **104**(44), 17494–17499 (2007)

M. Jacobs, R. Munje, B. Quadri, S. Muthukumar, S. Prasad, Tailoring of nanotextured zinc oxide thin films for enhanced biosensing. MRS Online Proceedings Library Archive **2014** (1690)

M. Jacobs, S. Muthukumar, A.P. Selvam, J.E. Craven, S. Prasad, Ultrasensitive electrical immunoassay biosensors using nanotextured zinc oxide thin films on printed circuit board platforms. Biosens. Bioelectron. **55**, 7–13 (2014)

V. Kamakoti, A. Panneer Selvam, N. Radha Shanmugam, S. Muthukumar, S. Prasad, Flexible molybdenum electrodes towards designing affinity based protein biosensors. Biosensors **6**(3), 36 (2016)

B. Kersten, A. Possling, F. Blaesing, E. Mirgorodskaya, J. Gobom, H. Seitz, Protein microarray technology and ultraviolet crosslinking combined with mass spectrometry for the analysis of protein–DNA interactions. Anal. Biochem. **331**(2), 303–313 (2004)

J.A. Lee, S. Hwang, J. Kwak, S.I. Park, S.S. Lee, K.-C. Lee, An electrochemical impedance biosensor with aptamer-modified pyrolyzed carbon electrode for label-free protein detection. Sensors Actuators B Chem. **129**(1), 372–379 (2008)

G.L. Liu, L.P. Lee, Nanowell surface enhanced Raman scattering arrays fabricated by soft-lithography for label-free biomolecular detections in integrated microfluidics. Appl. Phys. Lett. **87**(7), 074101 (2005)

G.L. Liu, Y.T. Rosa-Bauza, C.M. Salisbury, C. Craik, J.A. Ellman, F.F. Chen, L.P. Lee, Peptide-nanoparticle hybrid SERS probes for optical detection of protease activity. J. Nanosci. Nanotechnol. **7**(7), 2323–2330 (2007)

J.H.T. Luong, K.B. Male, J.D. Glennon, Biosensor technology: Technology push versus market pull. Biotechnol. Adv. **26**(5), 492–500 (2008)

R. Maalouf, C. Fournier-Wirth, J. Coste, H. Chebib, Y. Saïkali, O. Vittori, A. Errachid, J.-P. Cloarec, C. Martelet, N. Jaffrezic-Renault, Label-free detection of bacteria by electrochemical impedance spectroscopy: Comparison to surface plasmon resonance. Anal. Chem. **79**(13), 4879–4886 (2007)

B. Merriman, I.T. Team, J.M. Rothberg, Progress in ion torrent semiconductor chip based sequencing. Electrophoresis **33**(23), 3397–3417 (2012)

D.G. Myszka, X. He, M. Dembo, T.A. Morton, B. Goldstein, Extending the range of rate constants available from BIACORE: Interpreting

mass transport-influenced binding data. Biophys. J. **75**(2), 583–594 (1998)

A. Panneer Selvam, S. Prasad, Nanosensor electrical immunoassay for quantitative detection of NT-pro brain natriuretic peptide. Futur. Cardiol. **9**(1), 137–147 (2013)

Piliarik, M.; Vaisocherová, H.; Homola, J., Surface plasmon resonance biosensing. In Biosensors and Biodetection, Springer: 2009; pp 65–88

M.I. Prodromidis, Impedimetric immunosensors—A review. Electrochim. Acta **55**(14), 4227–4233 (2010)

S. Ray, G. Mehta, S. Srivastava, Label-free detection techniques for protein microarrays: Prospects, merits and challenges. Proteomics **10**(4), 731–748 (2010)

D. Sarkar, W. Liu, X. Xie, A.C. Anselmo, S. Mitragotri, K. Banerjee, MoS2 field-effect transistor for next-generation label-free biosensors. ACS Nano **8**(4), 3992–4003 (2014)

B. Schweitzer, P. Predki, M. Snyder, Microarrays to characterize protein interactions on a whole-proteome scale. Proteomics **3**(11), 2190–2199 (2003)

Selvam, A. P.; Vattipalli, K. M.; Prasad, S. In Design of a high sensitive non-faradaic impedimetric sensor, Engineering in Medicine and Biology Society (EMBC), 2012 Annual International Conference of the IEEE, IEEE: 2012; pp 3251–3254

N.R. Shanmugam, S. Muthukumar, A.P. Selvam, S. Prasad, Electrochemical nanostructured ZnO biosensor for ultrasensitive detection of cardiac troponin-T. Nanomedicine **11**(11), 1345–1358 (2016)

M.L.Y. Sin, K.E. Mach, P.K. Wong, J.C. Liao, Advances and challenges in biosensor-based diagnosis of infectious diseases. Expert. Rev. Mol. Diagn. **14**(2), 225–244 (2014)

N. Talukder, A. Furniturewalla, T. Le, M. Chan, S. Hirday, X. Cao, P. Xie, Z. Lin, A. Gholizadeh, S. Orbine, A portable battery powered microfluidic impedance cytometer with smartphone readout: Towards personal health monitoring. Biomed. Microdevices **19**(2), 36 (2017)

S.K. Tuteja, R. Chen, M. Kukkar, C.K. Song, R. Mutreja, S. Singh, A.K. Paul, H. Lee, K.-H. Kim, A. Deep, A label-free electrochemical immunosensor for the detection of cardiac marker using graphene quantum dots (GQDs). Biosens. Bioelectron. **86**, 548–556 (2016)

S. Umehara, M. Karhanek, R.W. Davis, N. Pourmand, Label-free biosensing with functionalized nanopipette probes. Proc. Natl. Acad. Sci. **106**(12), 4611–4616 (2009)

Q. Yu, G. Golden, Probing the protein orientation on charged self-assembled monolayers on gold nanohole arrays by SERS. Langmuir **23**(17), 8659–8662 (2007)

X. Yu, D. Xu, Q. Cheng, Label-free detection methods for protein microarrays. Proteomics **6**(20), 5493–5503 (2006)

G. Zheng, F. Patolsky, Y. Cui, W.U. Wang, C.M. Lieber, Multiplexed electrical detection of cancer markers with nanowire sensor arrays. Nat. Biotechnol. **23**(10), 1294–1301 (2005a)

G. Zheng, F. Patolsky, Y. Cui, W.U. Wang, C.M. Lieber, Multiplexed electrical detection of cancer markers with nanowire sensor arrays. Nat. Biotechnol. **23**(10), 1294 (2005b)